

Femtosecond Response of a Single Metal Nanoparticle

Otto L. Muskens, Natalia Del Fatti,* and Fabrice Vallée

Centre de Physique Moléculaire Optique et Hertzienne, CNRS and Université Bordeaux I, 351 cours de la Libération, 33405 Talence, France

Received December 6, 2005; Revised Manuscript Received January 12, 2006

ABSTRACT

The ultrafast nonlinear optical response of a single metal nanoparticle is investigated by combining a high-sensitivity femtosecond pump–probe setup with a spatial modulation microscope. Experiments are performed on 20 and 30 nm silver nanospheres, in situ characterized via their optical linear extinction spectrum. The measured transient response permits investigation of the electron–phonon energy transfer time in a single nanoparticle. Its dependence on the electronic temperature is quantitatively interpreted using the two-temperature model.

Time-resolved femtosecond spectroscopy has been extensively used to investigate the ultrafast nonlinear optical response and the correlated electronic and vibrational kinetics of nanoparticles and nanomaterials. In particular, it constitutes a powerful tool for analyzing electron interaction processes and their modification by size reduction in metal nanoparticles.^{1–4} Most of these experiments were performed on large ensembles of particles dispersed in a liquid or solid matrix, with the concomitant difficulty of nanoparticle size, shape, and environment fluctuations. In the case of nanospheres, this has been circumvented by using high-quality samples with weak size and shape dispersions and performing experiments in environment independent conditions (i.e., for weak excitation of the particles).^{5,6} However, precise investigation of the impact of the particle shape and environment on the electron response requires the development of femtosecond spectroscopy of single identified nanoparticles.

Time-resolved investigations of single metal nanoparticles of nanostructured metal surfaces rely on combining a specific optical detection scheme with a femtosecond spectroscopy setup.^{7–12} In the case of nanoparticles, near field optical microscopy has been recently extended to the femtosecond investigation of large gold nanorods (180 × 30 nm),⁷ using an approach similar to that developed for semiconductor nanostructures.^{13,14} The inherent difficulty of these experiments is making development of far field techniques particularly interesting. Though their spatial resolution is smaller, single nanoparticles can also be addressed using dilute samples. Transient single nanoparticle scattering and absorption have thus been detected in large nanospheres (diameter larger than 50 nm) with picosecond resolution.^{8,9} Scattering-based methods have recently been extended to the femtosecond domain in 80 nm gold nanospheres¹⁰ and in

nanorods.¹¹ As, for small nanoparticles, absorption dominates over scattering, transient absorption has to be monitored to address smaller particles (the ratio of the absorption to scattering cross sections scales as the particle volume). We report here on the first femtosecond investigation of the transient absorption of a single small metal nanoparticle (size smaller than 50 nm), coupling our recently demonstrated far-field spatial modulation spectroscopy technique¹⁵ with a high sensitivity pump–probe setup. This approach permits both to identify the studied particle via its linear extinction spectrum and to detect its ultrafast response, yielding information on the electron–lattice energy exchange in a single nanoparticle down to 20 nm size.

Experiments were performed in single silver nanospheres deposited on a cover glass. The samples were prepared by spin coating a colloidal solution in the presence of a polymer (poly(vinyl alcohol)). Two solutions with a mean diameter of 20 or 30 nm and a size dispersion of ±5 nm were used. With proper choice of the deposition conditions, very diluted samples were obtained, with less than one particle per μm^2 . The single particle under study was first identified by measuring its extinction spectrum using the spatial modulation spectroscopy technique.^{15,16} This is based on periodically modulating the position of a nanoparticle in the focal spot of a laser beam of wavelength λ tightly focused by a 100× microscope objective. The resulting modulation of the transmitted power is detected by a lock-in amplifier. Its amplitude is imposed by the nanoparticle extinction cross section, $\sigma_{\text{ext}}(\lambda)$, whose absolute value can thus be precisely determined. This setup permits detection of an absorbing nanoobject with an absorption cross section down to a few nm^2 , yielding a detection limit of 2 nm for silver nanospheres.¹⁵

* Corresponding author: n.delfatti@cpmoh.u-bordeaux1.fr.

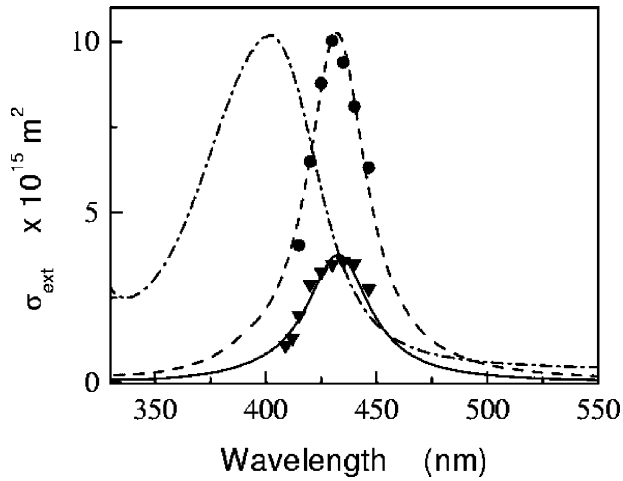


Figure 1. Measured extinction cross section of two single Ag nanoparticles (circles and triangles) deposited on a glass substrate in the presence of a polymer (poly(vinyl alcohol)). The solid and dashed lines are the spectra of a spherical particle of diameter $D = 21$ nm (triangles) and 30 nm (circles) computed using the Mie theory in the multipolar approximation. The dash-dotted line is the normalized ensemble absorption spectrum of the Ag colloidal solution with average size $\langle D \rangle = 20$ nm. The large displacement of the extinction peak is due to the change of the refractive index of the nanoparticle embedding medium (see text).

In the present experiments, the extinction spectrum and femtosecond transient absorption of a single nanoparticle were measured using the same homemade Ti:sapphire oscillator as light source. It delivers 100 fs pulses, tunable in the 800–900 nm spectral range at 76 MHz. The pulse train was separated into two parts, one of which being frequency doubled in a BBO crystal. For spectrum measurements, only the latter part was used providing a light source tunable in the 400–450 nm range, close to the silver particle surface plasmon resonance. For time-resolved experiments, both parts were used, as the pump and probe beams, respectively (see below).

Single absorption spectra of two silver nanoparticles are shown Figure 1 and compared to the ensemble spectrum of the colloidal aqueous solution with average diameter $\langle D \rangle = 20$ nm. Individual spectra show red shifted ($\lambda_R \approx 430$ nm) and narrowed surface plasmon resonances, as compared to the ensemble measurements performed in the colloidal solution ($\lambda_R \approx 400$ nm). The peak $\sigma_{\text{ext}}(\lambda_R)$ values of the studied single particles at the surface plasmon resonance wavelength are about 1×10^4 nm² and 3.7×10^3 nm².

Assuming spherical nanoparticles and an isotropic embedding medium of dielectric constant ϵ_m , the measured spectra can be reproduced using the Mie theory.¹⁷ At the lowest order (dipolar approximation) valid for a nanosphere of diameter D , much smaller than the optical wavelength, the extinction cross section σ_{ext} is given by

$$\sigma_{\text{ext}}(\lambda) = \frac{18\pi V \epsilon_m^{3/2}}{\lambda} \frac{\epsilon_2(\lambda)}{|\epsilon(\lambda) + 2\epsilon_m|^2} \quad (1)$$

where $\epsilon = \epsilon_1 + \epsilon_2$ is the dielectric function of the metal

nanoparticle of volume V . The observed displacement of the surface plasmon resonance wavelength λ_R from the solution to a deposited nanoparticle is consistent with the change of the particle environment (increase of ϵ_m in eq 1).¹⁷ For small particles in the dipolar approximation, λ_R is independent of the particle size for a fixed ϵ_m . This is consistent with the observed close position of the peak extinction for the two selected particles of Figure 1 (however, for these particles a more precise description requires inclusion of multipolar terms, see below). The much larger width of the surface plasmon resonance in ensemble measurements is ascribed to inhomogeneous broadening due to environment fluctuations from particle to particle.

As the absolute value of the extinction cross section is measured, comparison of the computed and measured spectra permits precise characterization of the studied single nanoparticle and, in particular, determination of its volume.¹⁶ Actually, already for $D \approx 20$ nm silver nanoparticles, the retardation effect influences the spectrum and has to be taken into account. It corresponds to including multipolar terms in the Mie theory (up to the 11th order in the present study). For the two particles of Figure 1 we obtain $D = 21$ and 30 nm, using the bulk ϵ values measured by Johnson and Christy,¹⁸ corrected for surface effect.¹⁷ For these particles, absorption dominates over scattering, the cross-section ratio $\sigma_{\text{abs}}/\sigma_{\text{sca}}$ at λ_R being about 10 for the former and 3 for the latter. For a given set of dielectric constant ϵ , a very precise determination of D is obtained with a ± 0.2 nm error. Actually the main uncertainty is due to the deviation of the ϵ values measured by different authors. For instance, very similar fitting can be performed with the ϵ data reported by Palik,¹⁹ yielding $D = 21$ and 31 nm. Including this systematic error, the overall precision on the D value can be estimated to be smaller than 1 nm.

Femtosecond pump–probe experiments were performed on these identified single nanoparticles using the same setup. The two femtosecond near-infrared and blue beams were now injected in the spatial modulation microscope. The individual nanoparticle is excited by absorption of the femtosecond near-infrared pulses ($\lambda_{\text{pp}} = 850$ nm). The induced transmission change $\Delta T/T$ is probed close to the surface plasmon resonance with the frequency doubled part of the pulse train at $\lambda_{\text{PR}} = 425$ nm. The use of this same beam in spectral and temporal measurements also permits precise alignment of the setup and control of any evolution of the studied particle through monitoring of its extinction spectrum. Both pump and probe beams were tightly focused on the single nanoparticle with Gaussian spots of full width at half-maximum 570 and 290 nm, respectively. The $\Delta T/T$ signal was monitored as a function of the pump–probe delay using a classical pump–probe setup. It uses mechanical chopping of the pump beam at 2 kHz and lock-in detection of the transmitted probe beam. Because of the excellent laser stability, high sensitivity is achieved with a noise level in the 10^{-6} range for $\Delta T/T$ measurements.

When a single nanoparticle is illuminated by a beam focused over an equivalent spot size, S_{PR} (top hat spatial profile of same energy), the sample transmission is given

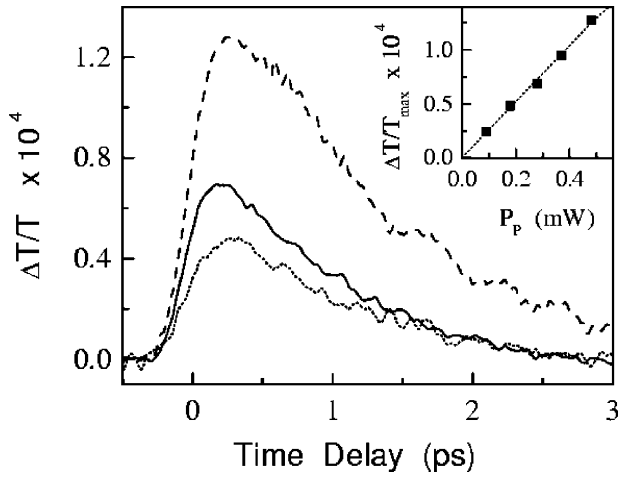


Figure 2. Temporal evolution of the transmission change $\Delta T/T$ measured in one single $D = 30$ nm Ag nanoparticle for different incident pump powers P_p : $180 \mu\text{W}$ (dotted line), $280 \mu\text{W}$ (solid line), and $480 \mu\text{W}$ (dashed line). The pump and probe wavelengths are $\lambda_{pp} = 850$ nm and $\lambda_{pr} = 425$ nm, respectively. The inset shows the measured linear dependence of the maximum signal amplitude on the pump power.

by $T \approx T_s(1 - \sigma_{\text{ext}}(\lambda_{\text{PR}})/S_{\text{PR}})$ where T_s is the transmission when no particle is under the focal spot. The pump-induced transmission change can thus be written

$$\Delta T/T \approx -(\Delta\sigma_{\text{ext}}/\sigma_{\text{ext}})(\sigma_{\text{ext}}/S_{\text{PR}}) \quad (2)$$

The first term is the relative modification of the extinction cross section induced by the pump pulse. It can be estimated from classical pump-probe experiments on nanoparticle ensembles. It depends on the amount of energy injected in the electron gas and varies from about 10^{-2} for strong excitation to typically 10^{-3} – 10^{-4} in the low perturbation regime (see below). The second term, proportional to the linear extinction of one nanoparticle, is the overall time-domain signal reduction factor due to probing a single object. For silver nanoparticles in the 20–30 nm range, it is of the order of 10^{-2} , leading to a $\Delta T/T$ signal in the 10^{-4} – 10^{-6} range, detectable by our apparatus.

The time evolution of the transmission change $\Delta T/T$ measured in the $D = 30$ nm silver nanoparticle is shown Figure 2 for three different pump powers. The $\Delta T/T$ amplitude is consistent with the estimated one and its maximum value is proportional to the pump excitation (Figure 2, inset), showing that two-photon absorption is negligible. The good signal over noise ratio of the data permits precise analysis of the $\Delta T/T$ time behavior and thus the electron kinetics it reflects.¹ In these experiments, absorption of an infrared pump pulse creates a strongly athermal conduction electron distribution that thermalizes by electron-electron scattering and cools down by electron-lattice coupling. In silver, for a probe pulse in the vicinity of the surface plasmon resonance, the ultrafast nonlinear response essentially reflects the time-dependent excess energy Δu_e of the electron gas, as previously reported and modeled for ensemble measurements.²⁰ Consequently, the $\Delta T/T$ signal rise follows energy injection and is limited by

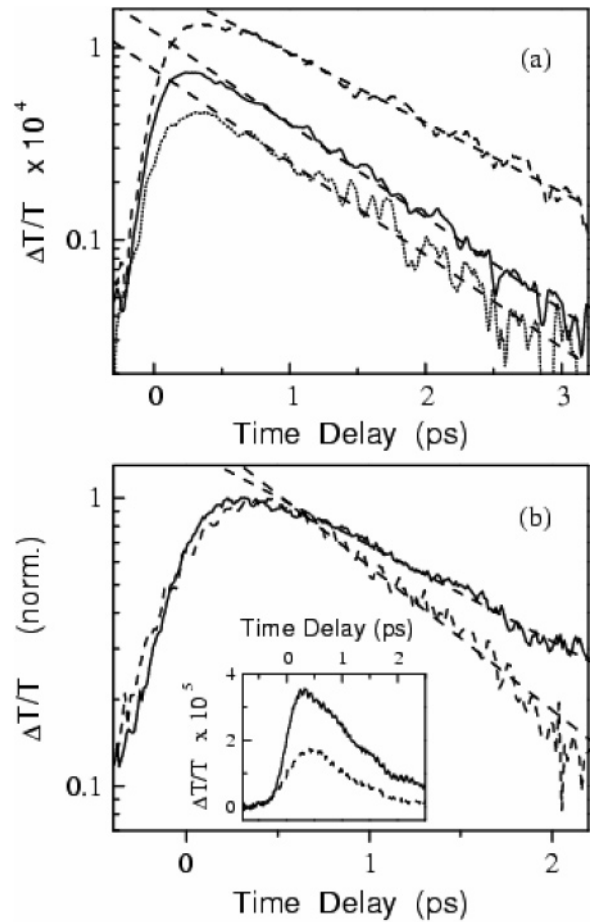


Figure 3. Time dependence of the transmission changes $\Delta T/T$ measured on single $D = 30$ nm (a) and 21 nm (b) silver nanoparticles, on a logarithmic scale. The pulse durations at the sample position are about (a) 140 fs and (b) 200 fs. The dashed straight lines correspond to exponential decays with (a) $\tau_{e-ph} = 1$ ps (dotted line data, $P_p \approx 180 \mu\text{W}$), 1.05 ps (solid line data, $280 \mu\text{W}$), and 1.3 ps (upper dashed line data, $480 \mu\text{W}$) and (b) $\tau_{e-ph} = 950$ fs (dashed line data, $150 \mu\text{W}$) and $\tau_{e-ph} = 1.3$ ps (solid line data, $300 \mu\text{W}$). The pump and probe wavelengths are (a) 850 and 425 nm and (b) 835 and 417 nm, respectively. The inset in (b) shows the transmission change $\Delta T/T$ on a linear scale.

the duration of the pulses. Its decay reflects the losses of the electron gas energy to the lattice that can thus be analyzed in a single particle.

For the different pump powers used here, almost exponential decays of $\Delta T/T$ are observed (Figure 3). Even for the lower excitation, the decay is followed over more than 1 decade yielding a time constant $\tau_{e-ph} \approx 900$ fs for the $D = 30$ nm particle (Figure 4). For higher pump energies, longer $\Delta T/T$ decay times are observed with $\tau_{e-ph} \approx 1.3$ ps for the largest energy. Similar results were obtained for the $D = 21$ nm nanoparticle, with a comparable energy transfer time τ_{e-ph} of 950 fs at low excitation that strongly increases with pump power (Figure 3b). The low-energy τ_{e-ph} values are consistent with the intrinsic electron-lattice energy transfer time, $\tau_{e-ph}^0 \approx 850$ fs, measured in a large ensemble of matrix embedded $D \approx 25$ nm nanoparticles (about 10^5) in the weak electron perturbation regime.⁶

The dependence of the energy transfer time on the pump power and its different behavior in the 21 and 30 nm particles

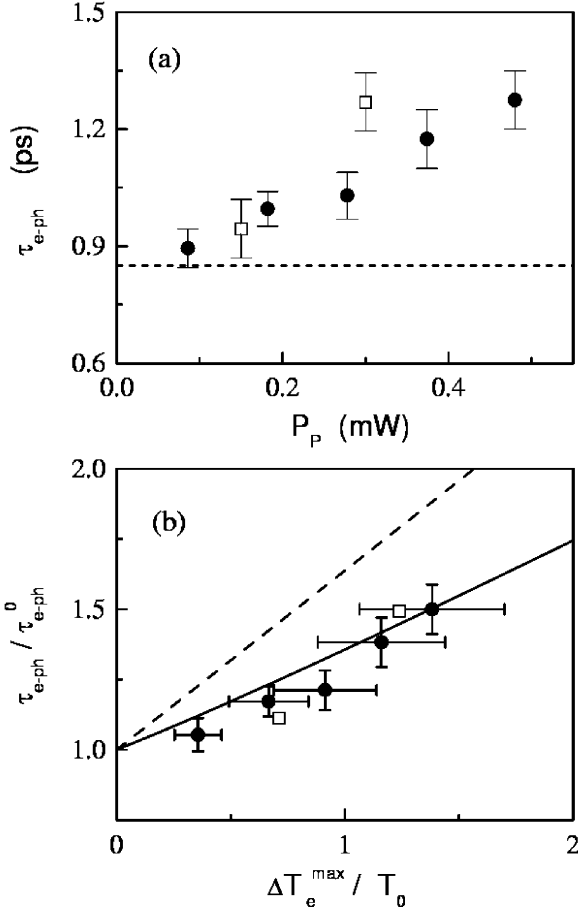


Figure 4. (a) Electron–phonon energy transfer time, τ_{e-ph} , measured for two single Ag nanoparticles ($D = 21$ nm, open squares, and $D = 30$ nm, closed circles) for different pump powers P_p . The dashed line is the electron–phonon energy transfer time, $\tau_{e-ph}^0 \approx 850$ fs, measured in an ensemble of silver nanoparticles with mean diameter 25 nm in the low perturbation regime.⁶ (b) Measured decay time τ_{e-ph} normalized to τ_{e-ph}^0 as a function of the initial temperature increase ΔT_e^{\max} . The dashed and full lines are the time τ_{T_e} , and τ_{u_e} , normalized to τ_{e-ph}^0 , for ΔT_e and Δu_e to decay by $1/e$, computed using eqs 4 and 5. The error bars for the 21 nm particle are not shown for clarity.

are ascribed to the electron excitation dependence of the electron–lattice energy transfer kinetics. After establishment of an electron temperature, i.e., a few hundred femtoseconds, the electron–lattice energy exchanges have been described in bulk metals using the two-temperature model²¹

$$\begin{cases} C_e(T_e) \frac{\partial T_e}{\partial t} = -G(T_e - T_L) \\ C_L \frac{\partial T_L}{\partial t} = G(T_e - T_L) \end{cases} \quad (3)$$

where T_e and T_L are the electron and lattice temperatures, C_e and C_L are their specific heat capacities, and G is the electron–phonon coupling constant. The electronic heat capacity is proportional to the electron temperature, $C_e(T_e) = c_0 T_e$ with $c_0 = 65$ J/(m³ K²) in silver. The electron excitation can be characterized by the maximum electron temperature rise induced by the pump pulse $\Delta T_e^{\max} = T_{\text{exc}}$

– T_0 , where T_0 is the initial temperature. In the weak perturbation regime, i.e., if ΔT_e^{\max} is small as compared to T_0 , the change of the electron heat capacity can be neglected. The electron temperature rise, $\Delta T_e(t)$ thus decays exponentially with the time constant $\tau_{e-ph}^0 \sim C_e(T_0)/G$ (eq 3). This is also the case for the electron excess energy

$$\Delta u_e = \frac{c_0}{2}(T_e^2 - T_0^2) \quad (4)$$

In contrast, for a strong excitation, the T_e dependence of C_e leads to a slower and excitation dependent decay of $\Delta T_e(t)$. The above rate equation system can be analytically solved,^{22,23} yielding for moderate metal heating ($T_e, T_L \ll 100$ K)

$$\frac{T_{\text{ext}} - T_e(t)}{T_f} - \ln \left[\frac{T_e(t) - T_f}{T_{\text{exc}} - T_f} \right] = \frac{G}{c_0 T_f} t \quad (5)$$

where T_f is the final temperature of the thermalized electron–lattice system that, because of the large lattice heat capacity ($C_L/C_e(T_0) \approx 100$ in silver), is close to T_0 . Though the predicted ΔT_e decay is not exponential,²⁴ it can still be approximated by an exponential if ΔT_e^{\max} does not exceed too much T_0 .²³ To compare the experimental and theoretical results, using eqs 4 and 5, we can define characteristic decay times τ_{T_e} , and τ_{u_e} , corresponding to the time for ΔT_e and Δu_e , respectively, to decay by $1/e$ (Figure 4).

This model can be generalized to metal nanoparticles down to a few nanometers in size for which quantum confinement effects weakly modify the electron properties. The key parameter in analyzing the observed electron energy kinetics is the excitation temperature T_{exc} . This is difficult to precisely define in ensemble measurements, because of the pump beam intensity profile at the focal spot and of the fluctuations of the absorption cross section of the nanoparticles due to their size, shape, and environment dispersion. This can be done in a single nanoparticle provided that, as here, it is in situ optically characterized. The amount of energy absorbed by the studied particle u_{abs} can be estimated using the absorption cross section at the pump wavelength. As this is too weak in the near-infrared region to be directly measured, it is calculated from the extinction spectra measured around the surface plasmon resonance using its fitting by the Mie theory (Figure 1). Taking into account electron energy losses to the lattice during the duration of the pump pulse, the effective maximum heating for the $D = 30$ nm nanoparticle is estimated to be in the 110–430 K range (Figure 4b). It depends on the set of bulk ϵ values, with the Johnson and Christy data yielding a larger electron temperature rise ΔT_e^{\max} than the Palik data. This uncertainty is mostly responsible for the large error bars for the ΔT_e^{\max} value (Figure 4b). For the $D = 21$ nm particle, excitation is larger for the same pump power, and ΔT_e^{\max} is estimated to vary from 220 to 380 K.

The decay times measured for a given electron temperature rise in the two studied particles are found to be in very good agreement with the predictions of the two temperature model

for the Δu_e kinetics (Figure 4b). This is consistent with the fact that for our probing conditions, the measured signal is proportional to Δu_e . The electron–phonon coupling constant, G (or equivalently τ_{e-ph}^0) measured in the bulk material has been used, confirming that it is weakly modified by size reduction for particles in the few tens of nanometer range.⁶

In conclusion, using a spatial modulation microscope coupled with a high sensitivity two-color femtosecond pump–probe setup, we have measured the ultrafast nonlinear response and the correlated electron kinetics of single small silver nanoparticles with sizes of 21 and of 30 nm. The use of the same apparatus for spectral and temporal measurements permits in situ optical identification of the studied nanoparticle. The electron–phonon energy transfer times deduced from the single particle time response can thus be quantitatively compared and are found in good agreement with the predictions of the two temperature model. These studies could be readily extended to smaller particles with diameter in the 10 nm range, for which size-dependent energy exchange kinetics has been demonstrated in ensemble measurements.⁵ This first femtosecond investigation of the transient absorption of a single metal nanoparticle opens up many possibilities for precise analysis of the ultrafast properties and electron kinetics of a metal nanoobject as a function of its size, shape, and environment.

Acknowledgment. The authors thank Conseil Régional d’Aquitaine for financial support.

References

- (1) Voisin, C.; Del Fatti, N.; Christofilos, D.; Vallée, F. *J. Phys. Chem. B* **2001**, *105*, 2264.
- (2) Halté, V.; Bigot, J. Y.; Palpant, B.; Broyer, M.; Prével, B.; Pérez, A. *Appl. Phys. Lett.* **1999**, *75*, 3799.
- (3) Hamanaka, Y.; Kuwabata, J.; Tanahashi, I.; Omi, S.; Nakamura, A. *Phys. Rev. B* **2001**, *63*, 104302.
- (4) Link, S.; Burda, C.; Mohamed, M. B.; Nikoobakht, B.; El-Sayed, M. A. *Phys. Rev. B* **2000**, *61*, 6086.

- (5) Voisin, C.; Christofilos, D.; Del Fatti, N.; Vallée, F.; Prével, B.; Cottancin, E.; Lermé, J.; Pellarin, M.; Broyer, M. *Phys. Rev. Lett.* **2000**, *85*, 2200. Voisin, C.; Christofilos, D.; Loukakos, P. A.; Del Fatti, N.; Vallée, F.; Lermé, J.; Gaudry, M.; Cottancin, E.; Pellarin, M.; Broyer, M. *Phys. Rev. B* **2004**, *69*, 195416.
- (6) Arbouet, A.; Voisin, C.; Christofilos, D.; Langot, P.; Del Fatti, N.; Vallée, F.; Lermé, J.; Celep, G.; Cottancin, E.; Gaudry, M.; Pellarin, M.; Broyer, M.; Maillard, M.; Pileni, M. P.; Treguer, M. *Phys. Rev. Lett.* **2003**, *90*, 177401.
- (7) Imura, K.; Nagahara, T.; Okamoto, H. *J. Phys. Chem. B* **2004**, *108*, 16344.
- (8) Matsuo, Y.; Sasaki, K. *Jpn. J. Appl. Phys.* **2001**, *40*, 6143.
- (9) van Dijk, M. A.; Lippitz, M.; Orrit, M.; cond-mat/0506401.
- (10) Itoh, T.; Asahi, T.; Masuhara, H. *Appl. Phys. Lett.* **2001**, *79*, 1667.
- (11) Pelton, M.; Liu, M.; Park, S.; Scherer, N.; Guyot-Sionnest, P. *SPIE Proc.* **2005**, *5927*, 59270Z.
- (12) Kubo, A.; Onda, K.; Petek, H.; Sun, Z.; Jung, Y. S.; Kim, H. K. *Nano Lett.* **2005**, *5*, 1123.
- (13) Nechay, B. A.; Siegner, U.; Morier-Genoud, F.; Schertel, A.; Keller, U. *Appl. Phys. Lett.* **1999**, *74*, 61.
- (14) Guenther, T.; Emiliani, V.; Intonti, F.; Lienau, C.; Elsaesser, T.; Nötzel, R.; Ploog, K. H. *Appl. Phys. Lett.* **1999**, *75*, 3500.
- (15) Arbouet, A.; Christofilos, D.; Del Fatti, N.; Vallée, F.; Huntzinger, J.-R.; Arnaud, L.; Billaud, P.; Broyer, M. *Phys. Rev. Lett.* **2004**, *93*, 127401.
- (16) Muskens, O.; Del Fatti, N.; Vallée, F. *SPIE Proc.* **2005**, *5927*, 59270Z.
- (17) Kreibitz, U.; Vollmer, M. *Optical Properties of Metal Clusters*; Springer: Berlin, 1995.
- (18) Johnson, P. B.; Christy, R. W. *Phys. Rev. B* **1972**, *6*, 4370.
- (19) Palik, E. D. *Handbook of Optical Constants of Solids*; Academic Press: New York, 1985.
- (20) Del Fatti, N.; Vallée, F.; Flytzanis, C.; Hamanaka, Y.; Nakamura, A. *Chem. Phys.* **2000**, *251*, 215.
- (21) Kaganov, M. I.; Lifshitz, I. M.; Tanatarov, L. V. *Sov. Phys. JETP* **1957**, *4*, 173.
- (22) Brorson, S. D.; Kazeroonian, A.; Modera, J. S.; Face, D. W.; Cheng, T. K.; Ippen, E. P.; Dresselhaus, M. S.; Dresselhaus, G. *Phys. Rev. Lett.* **1990**, *64*, 2172.
- (23) Vallée, F. In *Non-Equilibrium Dynamics of Semiconductors and Nanostructures*; Tsen, K. T., Ed.; CRC Press: New York, 2005; p 101.
- (24) Del Fatti, N.; Voisin, C.; Achermann, M.; Tzortzakis, S.; Christofilos, D.; Vallée, F. *Phys. Rev. B* **2000**, *61*, 16956.

NL0524086